

Dinuclear silver(I) complexes with pyridine-based macrocyclic type of ligand as antimicrobial agents against clinically relevant species: the influence of counter anion on the structure diversification of the complexes

Nada D. Savić,^{a*} Branka B. Petković,^b Sandra Vojnovic,^c Marija Mojicevic,^c Hubert Wadepohl,^d Kayode Olaifa,^e Enrico Marsili,^e Jasmina Nikodinovic-Runic,^c Miloš I. Djuran,^f and Biljana Đ. Glišić^{g*}

^aUniversity of Kragujevac, Institute for Information Technologies Kragujevac, Department of Science, Jovana Cvijića bb, 34000 Kragujevac, Serbia

^bUniversity of Priština-Kosovska Mitrovica, Faculty of Sciences, Lole Ribara 29, 38220 Kosovska Mitrovica, Serbia

^cInstitute of Molecular Genetics and Genetic Engineering, University of Belgrade, Vojvode Stepe 444a, 11042 Belgrade, Serbia

^dAnorganisch-Chemisches Institut, University of Heidelberg, Im Neuenheimer Feld 270, 69120 Heidelberg, Germany

^eDepartment of Chemical and Materials Engineering, Nazarbayev University, 53 Kabanbay Batyr Avenue, Nur-Sultan 010000, Kazakhstan

^fSerbian Academy of Sciences and Arts, Knez Mihailova 35, 11000 Belgrade, Serbia

^gUniversity of Kragujevac, Faculty of Science, Department of Chemistry, R. Domanovića 12, 34000 Kragujevac, Serbia

*Corresponding authors: Tel.: +381 34 336 223 (N. D. Savić); Tel.: +381 34 336 223 (B. Đ. Glišić).
E-mail addresses: nada.savic@kg.ac.rs (N. D. Savić); biljana.glisic@pmf.kg.ac.rs (B. Đ. Glišić).

Abstract

New dinuclear silver(i) complexes with *N,N',N'',N'''*-tetrakis(2-pyridylmethyl)-1,4,8,11-tetraazacyclotetradecane (tpmc), $[\text{Ag}_2(\text{NO}_3)(\text{tpmc})]\text{NO}_3 \cdot 1.7\text{H}_2\text{O}$ (**1**), $[\text{Ag}_2(\text{CF}_3\text{SO}_3)_2(\text{tpmc})]$ (**2**), and $[\text{Ag}_2(\text{tpmc})](\text{BF}_4)_2$ (**3**) were synthesized and characterized by NMR (^1H and ^{13}C), IR and UV-Vis spectroscopy, cyclic voltammetry and molar conductivity measurements. The molecular structures of the complexes were determined by single-crystal X-ray diffraction analysis. The spectroscopic and crystallographic data showed that the structure of the complexes strongly depends on the nature of the counteranion of silver(i) salt used for their synthesis. The antimicrobial activity of complexes **1–3** was examined against Gram-positive and Gram-negative bacteria and different species of unicellular fungus *Candida* spp. The ability of these complexes to inhibit the formation of *Candida* biofilms and to eradicate the already formed biofilms was tested in the standard microtiter plate-based assay. In addition, a bioelectrochemical testing of the antimicrobial activity of complex **1** against early biofilm was also performed. The obtained results indicated that complexes **1–3** showed increased activity toward Gram-negative bacteria and *Candida* spp. and could inhibit the formation of biofilms. In most cases, these complexes had positive selectivity indices and showed similar or even better activity with respect to the clinically used silver(i) sulfadiazine (AgSD). The values of the binding constants for complexes **1–3** to bovine serum albumin (BSA) were found to be high enough to indicate their binding to this biomolecule, but not so high as to prevent their release upon arrival at the target site. Moreover, the positive values of partition coefficients for these complexes indicated their ability to be transported through the cell membrane. Once inside the cell, complexes **1–3** could induce the formation of the reactive oxygen species (ROS) in *C. albicans* cells and/or interact with DNA. Taken together, silver(i) complexes with the tpmc ligand could be considered as novel antimicrobial compounds with favourable pharmacological properties, being safer than AgSD.

Keywords: Silver(I) complexes; Pyridine-based macrocycles; Antimicrobial activity; Biofilms; DNA/BSA interactions; Lipophilicity

TABLE OF CONTENTS

Fig. S1. Stability of complex 2 over time followed by UV-Vis spectrophotometry at 25 °C in (A) DMSO/H ₂ O, (B) DMSO/RPMI containing 2% of glucose and (C) DMSO/PBS.	S6
Fig. S2 Air/light stability of silver(I) complexes 1 – 3 .	S7
Fig. S3 Growth curves for selected strains at different [Fe(CN) ₆] ³⁻ concentrations (0 – 500 μM). (A) <i>C. parapsilosis</i> ATCC 22019; (B) <i>C. albicans</i> ATCC 10231; (C) <i>A. baumannii</i> ATCC 19606. Results show that 100 μM [Fe(CN) ₆] ³⁻ does not affect significantly the growth of both fungal and bacterial strains tested. Each dataset shows the average and standard deviation of three independent biological replicates (n = 3).	S8
Fig. S4 Charge output (Q) produced by biofilms when grown with and without [Fe(CN) ₆] ³⁻ as redox mediator for <i>A. baumannii</i> (ATCC 19606) (violet bar), <i>C. albicans</i> (ATCC 10231) (blue bar), <i>C. albicans</i> isolate 24 (black bar) and <i>C. parapsilosis</i> (ATCC 22019) (red bar). Results are the average of two independent biological replicates.	S9
Fig. S5 Effect of complex 1 on early biofilm of <i>C. parapsilosis</i> grown in the potentiostat-controlled bioelectrochemical cells. (A) Chronoamperometry (CA) of cells with 100 μM [Fe(CN) ₆] ³⁻ as redox mediator (black trace); cells with 100 μM [Fe(CN) ₆] ³⁻ and DMSO (red trace); cells with 100 μM [Fe(CN) ₆] ³⁻ and 0.9 μM of complex 1 dissolved in DMSO (blue trace). Cells with complex 1 dissolved in DMSO without redox mediator [Fe(CN) ₆] ³⁻ (green trace). (B) Cyclic voltammogram (CV) at 1 mV s ⁻¹ of <i>C. parapsilosis</i> at 0 h (dashed traces) and after 24 h (solid traces). Cells with 100 μM [Fe(CN) ₆] ³⁻ (black trace); cells with 100 μM [Fe(CN) ₆] ³⁻ and 0.9 μM of complex 1 dissolved in DMSO (blue traces). CA results are the	S10

average of two independent biological replicates. CV results are representative of two independent biological replicates.

Fig. S6 (A) Biofilm concentration measured with crystal violet assay for the four S11 strains *A. baumannii* (ATCC 19606), *C. albicans* (ATCC 10231), *C. albicans* 24 and *C. parapsilosis* (ATCC 22019). Cells with 100 μM $[\text{Fe}(\text{CN})_6]^{3-}$ (black bars); Cells with 100 μM $[\text{Fe}(\text{CN})_6]^{3-}$ and DMSO (green bars); Cells with 100 μM $[\text{Fe}(\text{CN})_6]^{3-}$ and the MIC concentration of **1** in planktonic culture (1.7, 2.1, 1.1, 0.9 μM for *A. baumannii* 19606, *C. albicans* 10231, *C. albicans* 24, *C. parapsilosis* 22019, respectively) dissolved in DMSO (red bars). Cells with **1** dissolved in DMSO (blue bars). The results are statistically significant for *A. baumannii* 19606 and *C. parapsilosis* 22019, with lower biofilm production in the presence of complex **1**. Results are the average of two independent biological replicates. **(B)** Optical density of planktonic cells after 24 h growth at $E = 0.4 \text{ V vs Ag}$ pseudo-reference electrode. Cells with mediator only (black); cells with mediator + DMSO (violet); cells with mediator + complex **1** (red); cells with complex **1** (blue). Results are the average of two independent biological replicates.

Fig. S7 (A) Fluorescence emission spectra of BSA in the absence and presence of S13 the silver(I) complexes **1** and **2** in PBS at 25 °C. Arrow shows the change upon increasing concentration of complex. **(B)** Stern-Volmer plots of relative BSA fluorescence intensity F_0/F vs [complex].

Fig. S8 Plots of $\log(F_0 - F)/F$ vs $\log[\text{complex}]$ for BSA interactions. S14

Fig. S9 (A) Fluorescence emission spectra of EthBr bound to DNA in the absence S15 and presence of the silver(I) complexes **2** and **3** in PBS at 25 °C. **(B)** Stern-Volmer plots of relative EthBr-DNA fluorescence intensity F_0/F vs [complex].

Fig. S10 Plots of $\log(F_0 - F)/F$ vs $\log[\text{complex}]$ for DNA interactions. S16

Fig. S11 CV voltammograms of complexes **2** and **3** after addition of increasing S17
concentration of DNA.

Table S1 Selected bond distances (\AA) and valence angles ($^\circ$) in silver(I) complexes S18
1 – 3.

Table S2 Minimal biofilm inhibition (MBIC) and eradication concentrations S20
(MBEC) of complexes **1** and **3**, μM (comparison between crystal violet and
tetrazolium salt (XTT) assay is presented)

Table S3 Details of the crystal structure determinations of the silver(I) complexes S21
1 – 3.

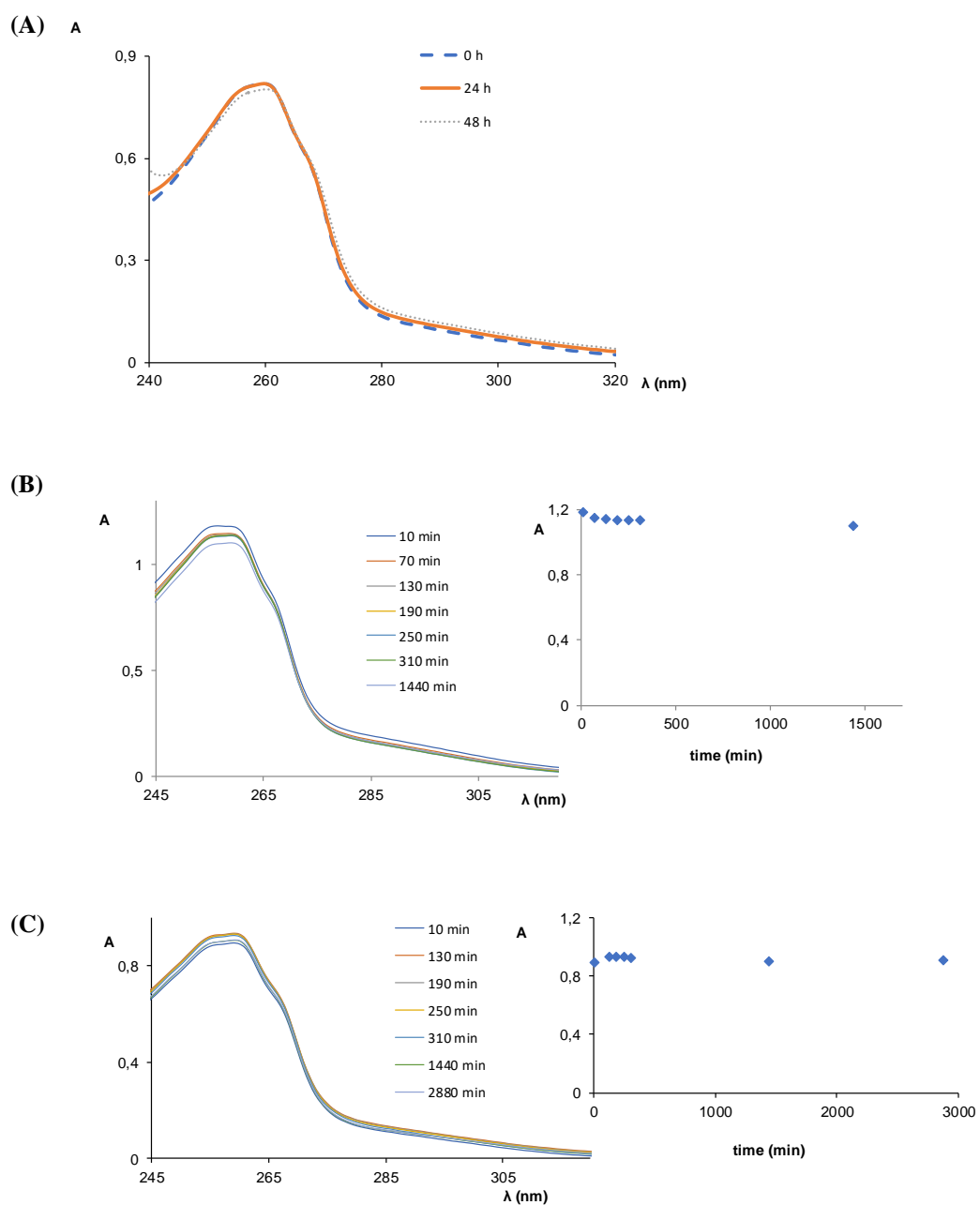


Fig. S1. Stability of complex **2** over time followed by UV-Vis spectrophotometry at 25 °C in (A) DMSO/H₂O, (B) DMSO/RPMI containing 2% of glucose and (C) DMSO/PBS.

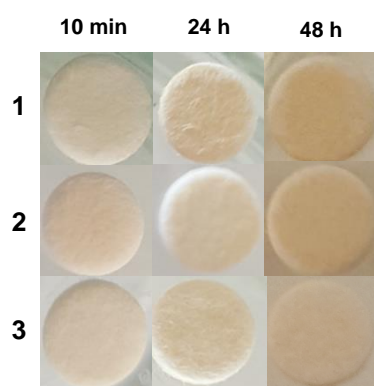


Fig. S2 Air/light stability of silver(I) complexes **1 – 3**.

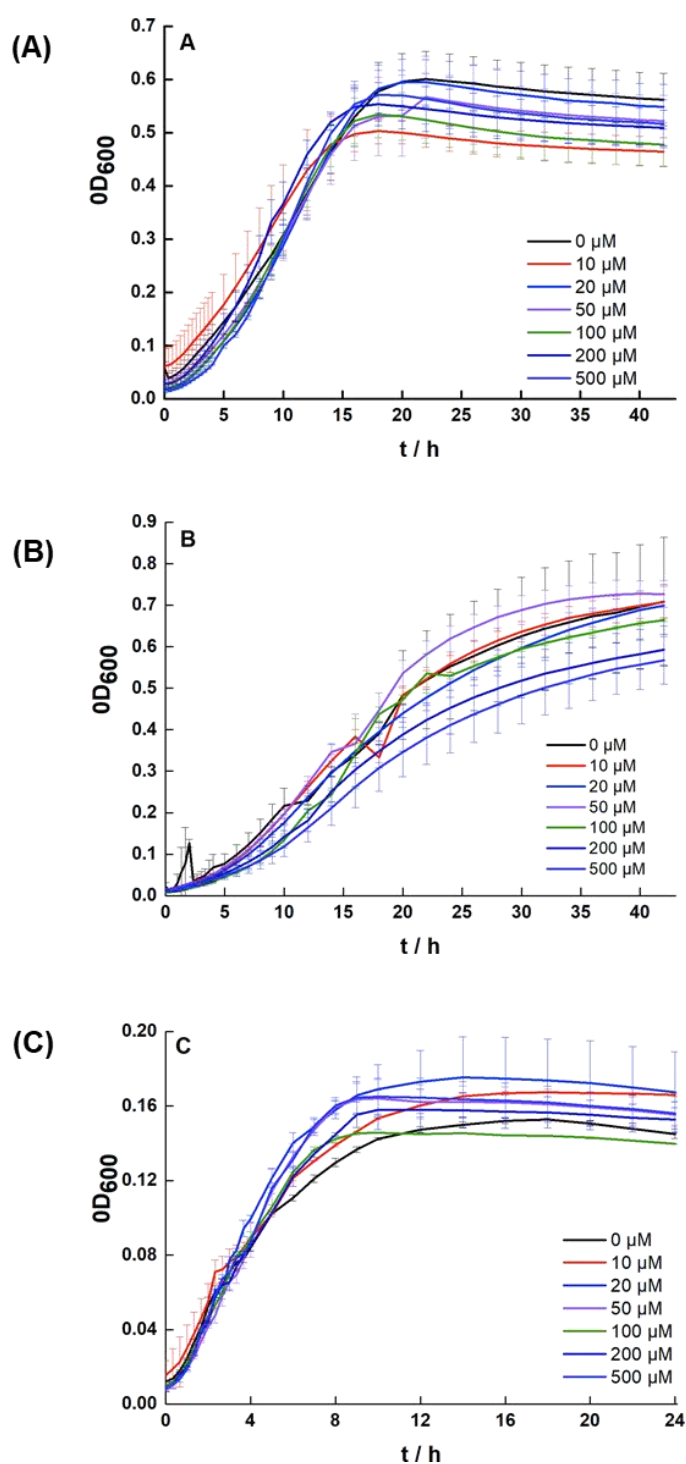


Fig. S3 Growth curves for selected strains at different $[\text{Fe}(\text{CN})_6]^{3-}$ concentrations (0 – 500 μM). (A) *C. parapsilosis* ATCC 22019; (B) *C. albicans* ATTC 10231; (C) *A. baumannii* ATCC 19606. Results show that 100 μM $[\text{Fe}(\text{CN})_6]^{3-}$ does not affect significantly the growth of both fungal and bacterial strains tested. Each dataset shows the average and standard deviation of three independent biological replicates ($n = 3$).

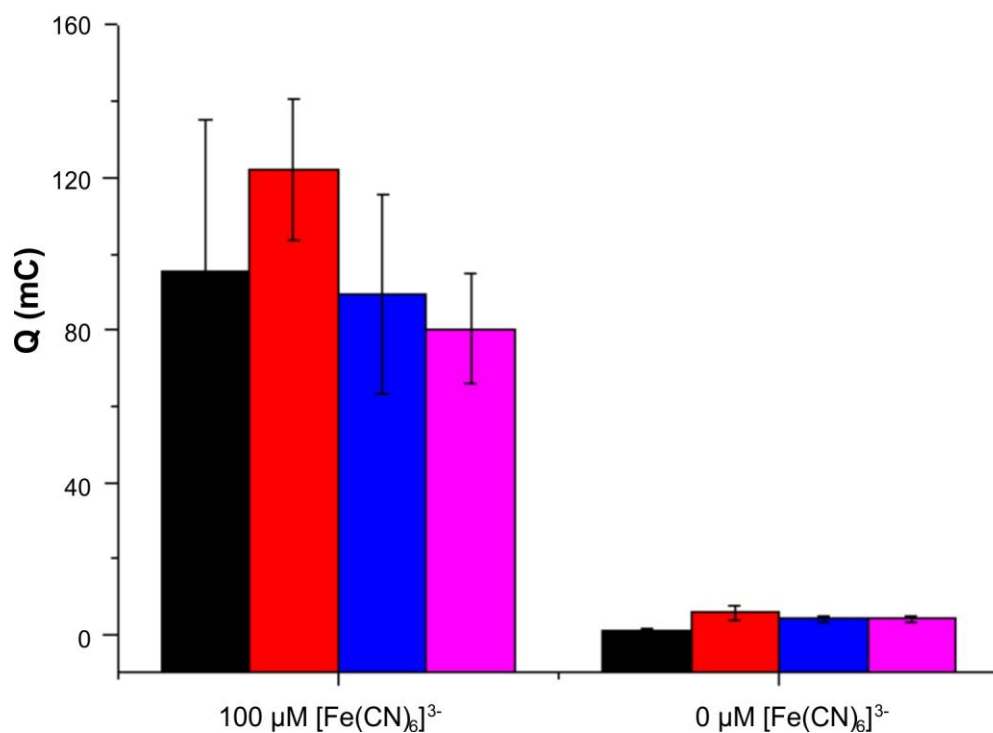


Fig. S4 Charge output (Q) produced by biofilms when grown with and without $[\text{Fe}(\text{CN})_6]^{3-}$ as redox mediator for *A. baumannii* (ATCC 19606) (violet bar), *C. albicans* (ATCC 10231) (blue bar), *C. albicans* isolate 24 (black bar) and *C. parapsilosis* (ATCC 22019) (red bar). Results are the average of two independent biological replicates.

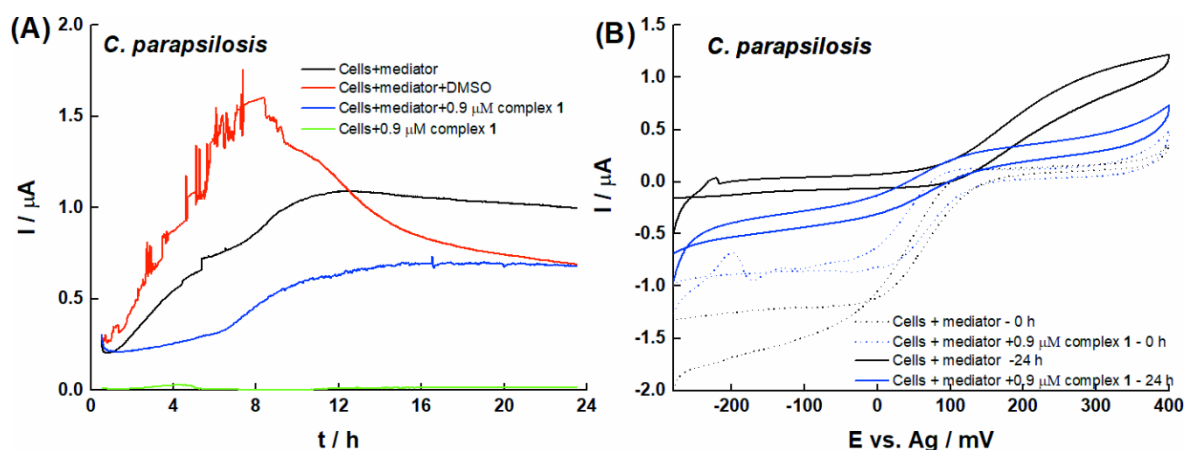


Fig. S5 Effect of complex 1 on early biofilm of *C. parapsilosis* grown in the potentiostat-controlled bioelectrochemical cells. (A) Chronoamperometry (CA) of cells with 100 μM $[\text{Fe}(\text{CN})_6]^{3-}$ as redox mediator (black trace); cells with 100 μM $[\text{Fe}(\text{CN})_6]^{3-}$ and DMSO (red trace); cells with 100 μM $[\text{Fe}(\text{CN})_6]^{3-}$ and 0.9 μM of complex 1 dissolved in DMSO (blue trace). Cells with complex 1 dissolved in DMSO without redox mediator $[\text{Fe}(\text{CN})_6]^{3-}$ (green trace). (B) Cyclic voltammogram (CV) at 1 mV s^{-1} of *C. parapsilosis* at 0 h (dashed traces) and after 24 h (solid traces). Cells with 100 μM $[\text{Fe}(\text{CN})_6]^{3-}$ (black trace); cells with 100 μM $[\text{Fe}(\text{CN})_6]^{3-}$ and 0.9 μM of complex 1 dissolved in DMSO (blue traces). CA results are the average of two independent biological replicates. CV results are representative of two independent biological replicates.

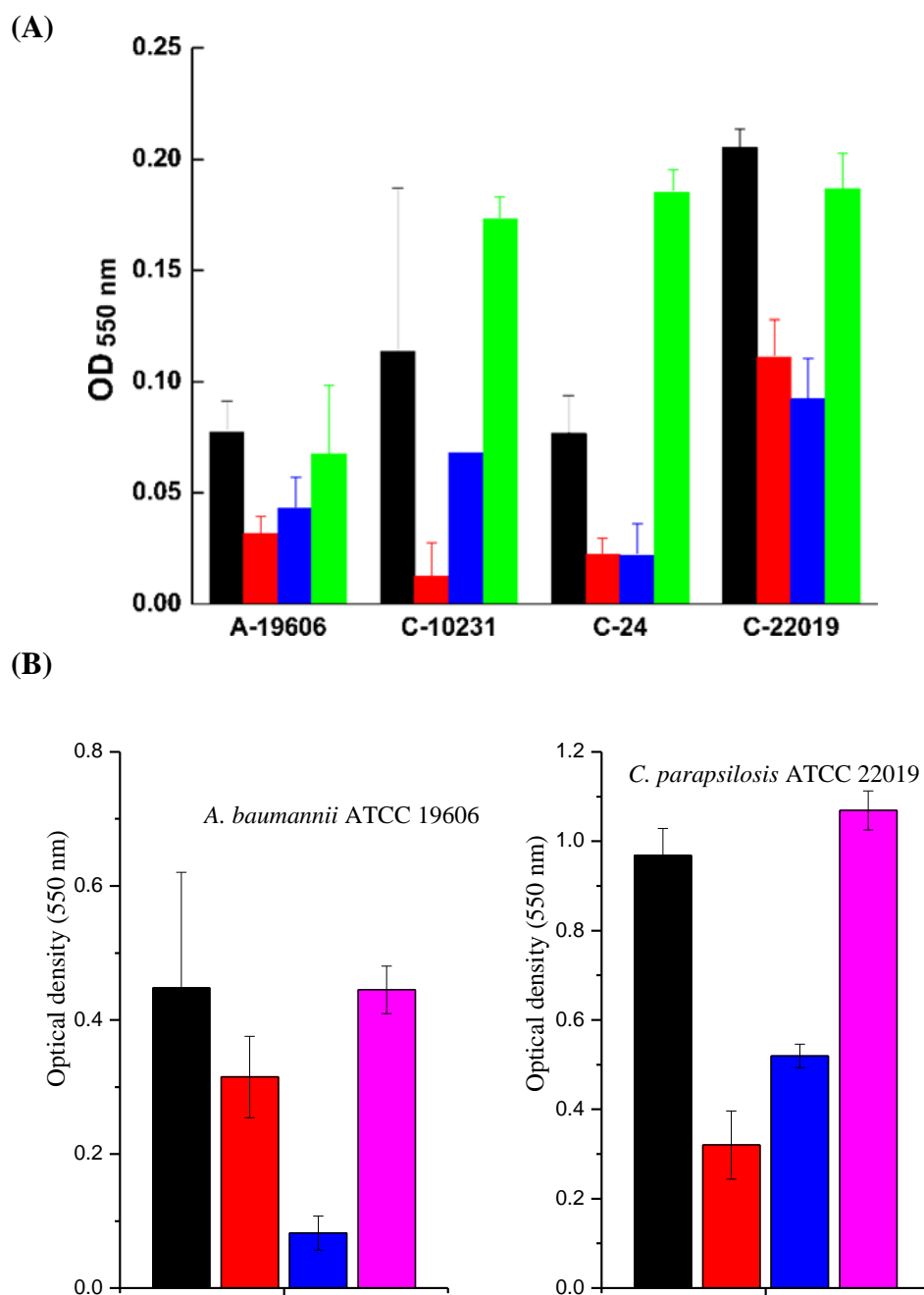


Fig. S6 (A) Biofilm concentration measured with crystal violet assay for the four strains *A. baumannii* (ATCC 19606), *C. albicans* (ATCC 10231), *C. albicans* 24 and *C. parapsilosis* (ATCC 22019). Cells with 100 μM $[\text{Fe}(\text{CN})_6]^{3-}$ (black bars); Cells with 100 μM $[\text{Fe}(\text{CN})_6]^{3-}$ and DMSO (green bars); Cells with 100 μM $[\text{Fe}(\text{CN})_6]^{3-}$ and the MIC concentration of **1** in planktonic culture (1.7, 2.1, 1.1, 0.9 μM for *A. baumannii* 19606, *C. albicans* 10231, *C. albicans* 24, *C. parapsilosis* 22019, respectively) dissolved in DMSO (red bars). Cells with

1 dissolved in DMSO (blue bars). The results are statistically significant for *A. baumannii* 19606 and *C. parapsilosis* 22019, with lower biofilm production in the presence of complex **1**. Results are the average of two independent biological replicates. **(B)** Optical density of planktonic cells after 24 h growth at $E = 0.4 \text{ V vs Ag}$ pseudo-reference electrode. Cells with mediator only (black); cells with mediator + DMSO (violet); cells with mediator + complex **1** (red); cells with complex **1** (blue). Results are the average of two independent biological replicates.

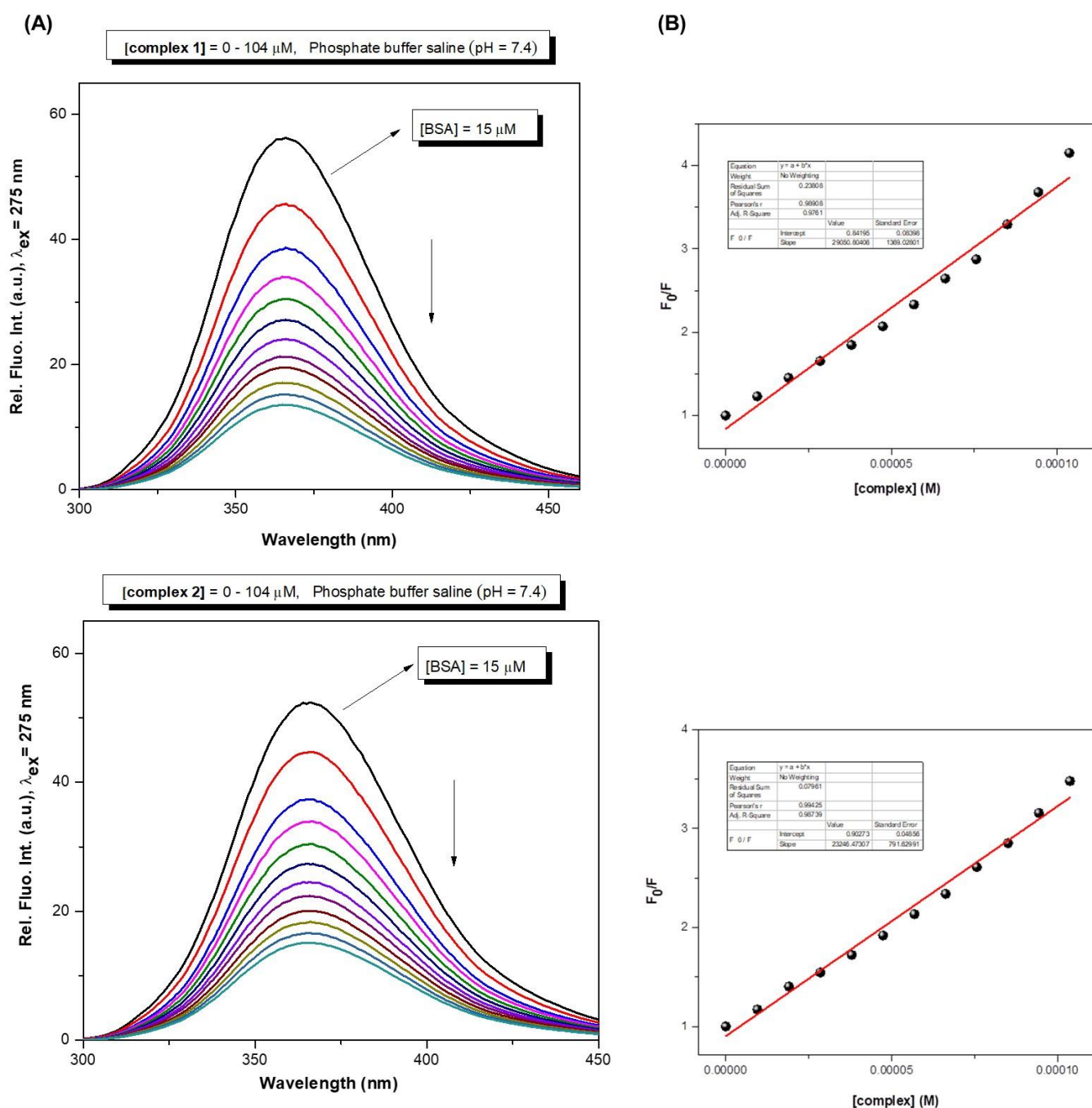


Fig. S7 (A) Fluorescence emission spectra of BSA in the absence and presence of the silver(I) complexes **1** and **2** in PBS at 25 °C. Arrow shows the change upon increasing concentration of complex. **(B)** Stern-Volmer plots of relative BSA fluorescence intensity F_0/F vs [complex].

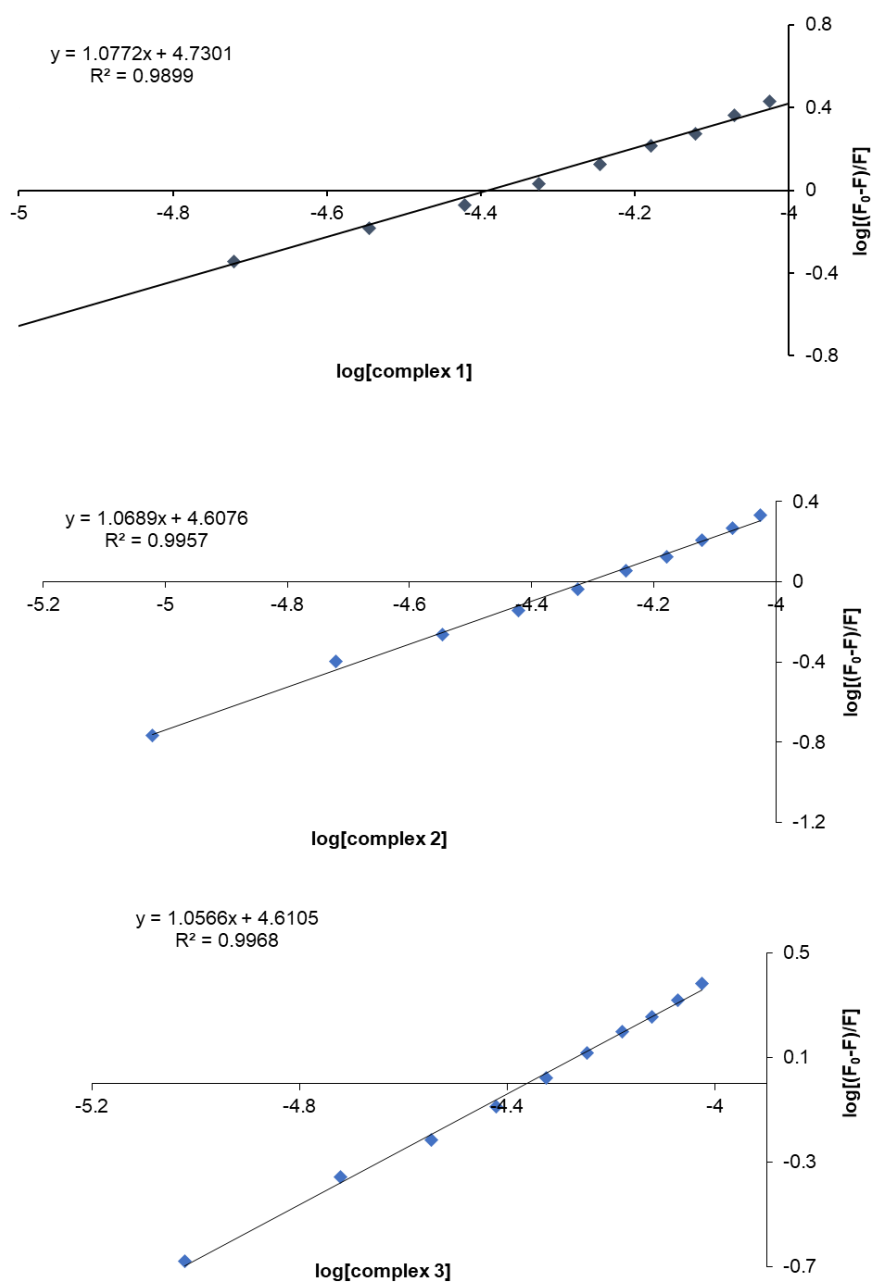


Fig. S8 Plots of $\log(F_0 - F)/F$ vs $\log[\text{complex}]$ for BSA interactions.

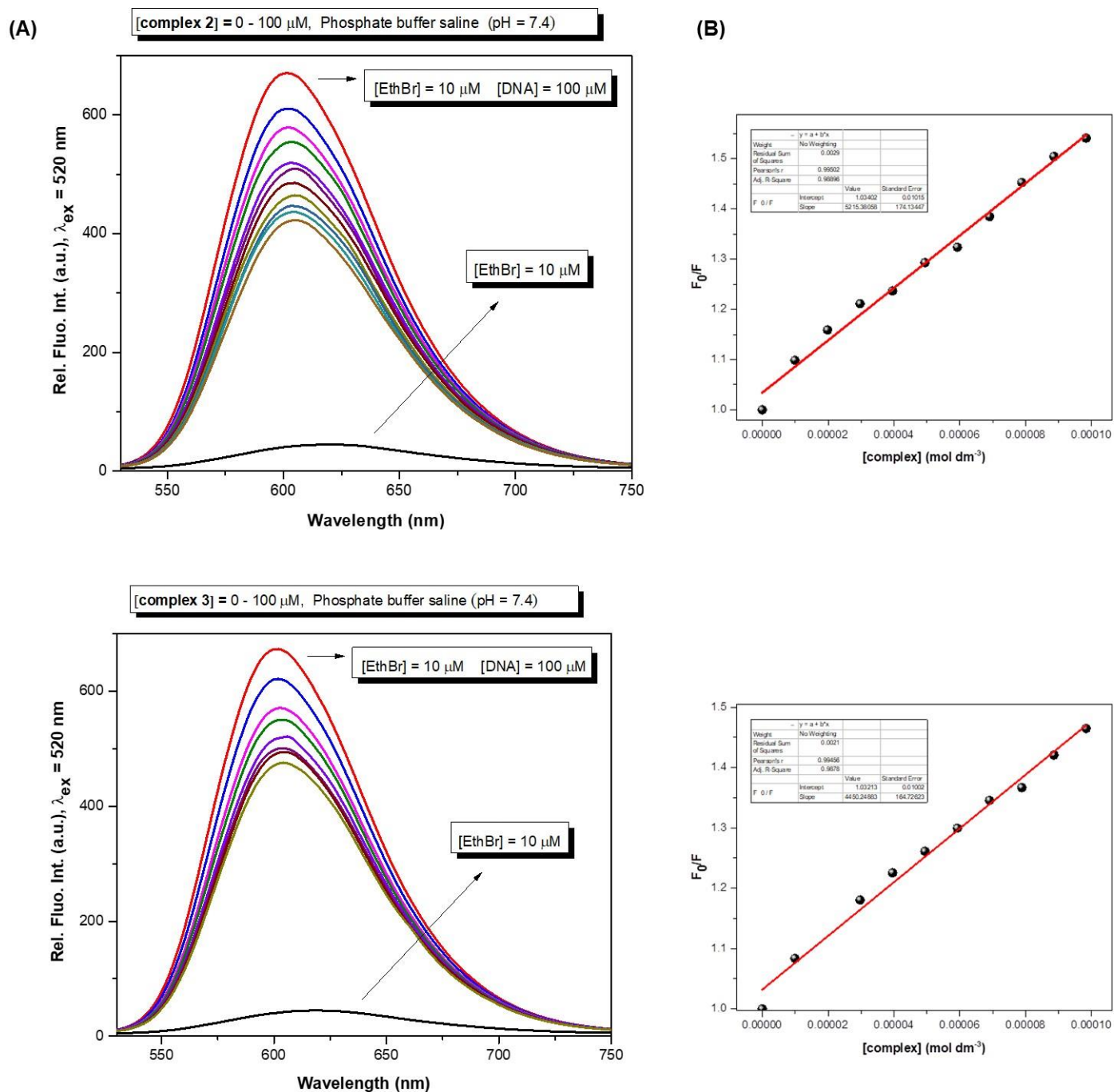


Fig. S9 (A) Fluorescence emission spectra of EthBr bound to DNA in the absence and presence of the silver(I) complexes **2** and **3** in PBS at 25 °C. (B) Stern-Volmer plots of relative EthBr-DNA fluorescence intensity F_0/F vs [complex].

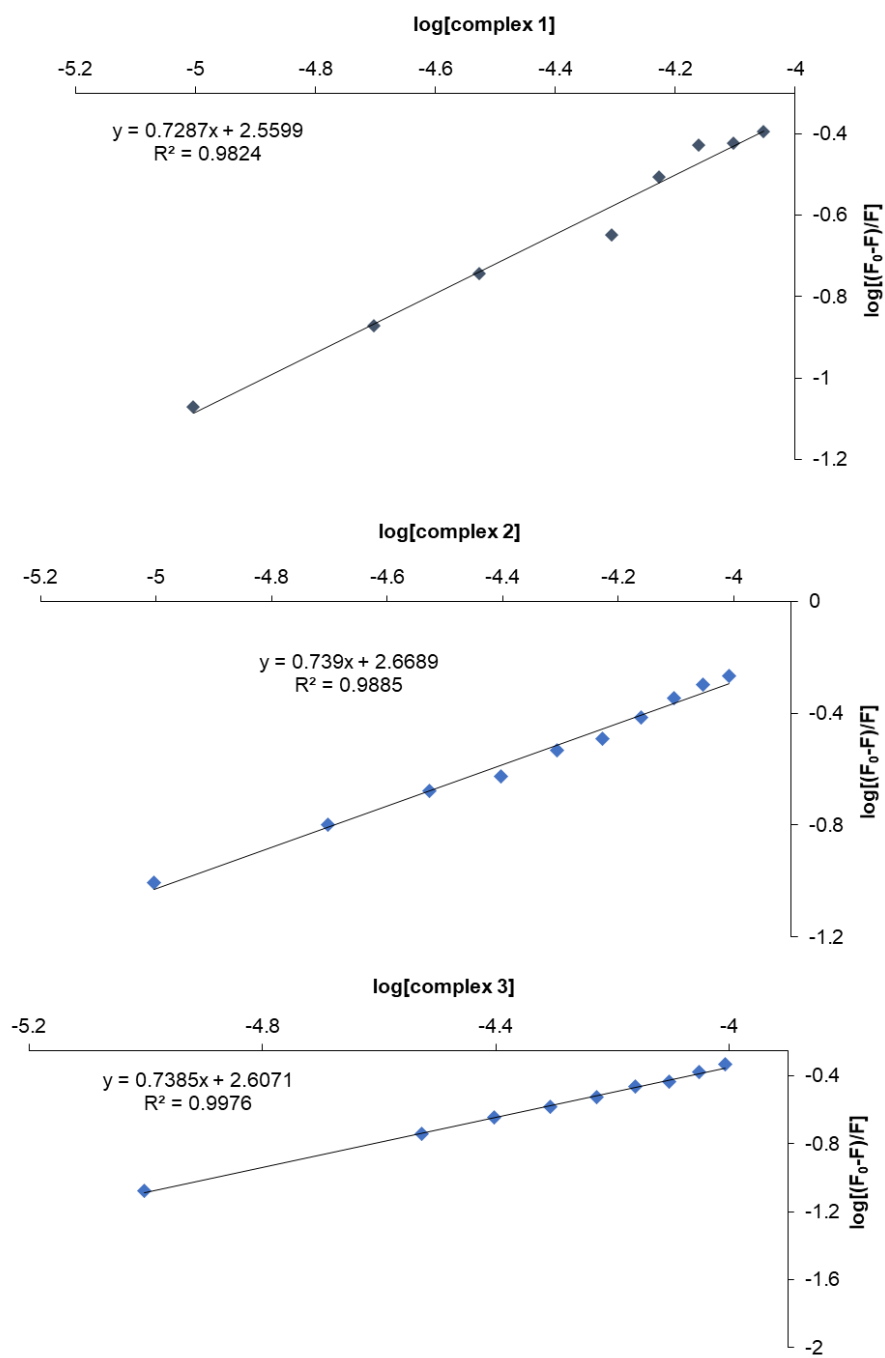


Fig. S10 Plots of $\log(F_0 - F)/F$ vs $\log[\text{complex}]$ for DNA interactions.

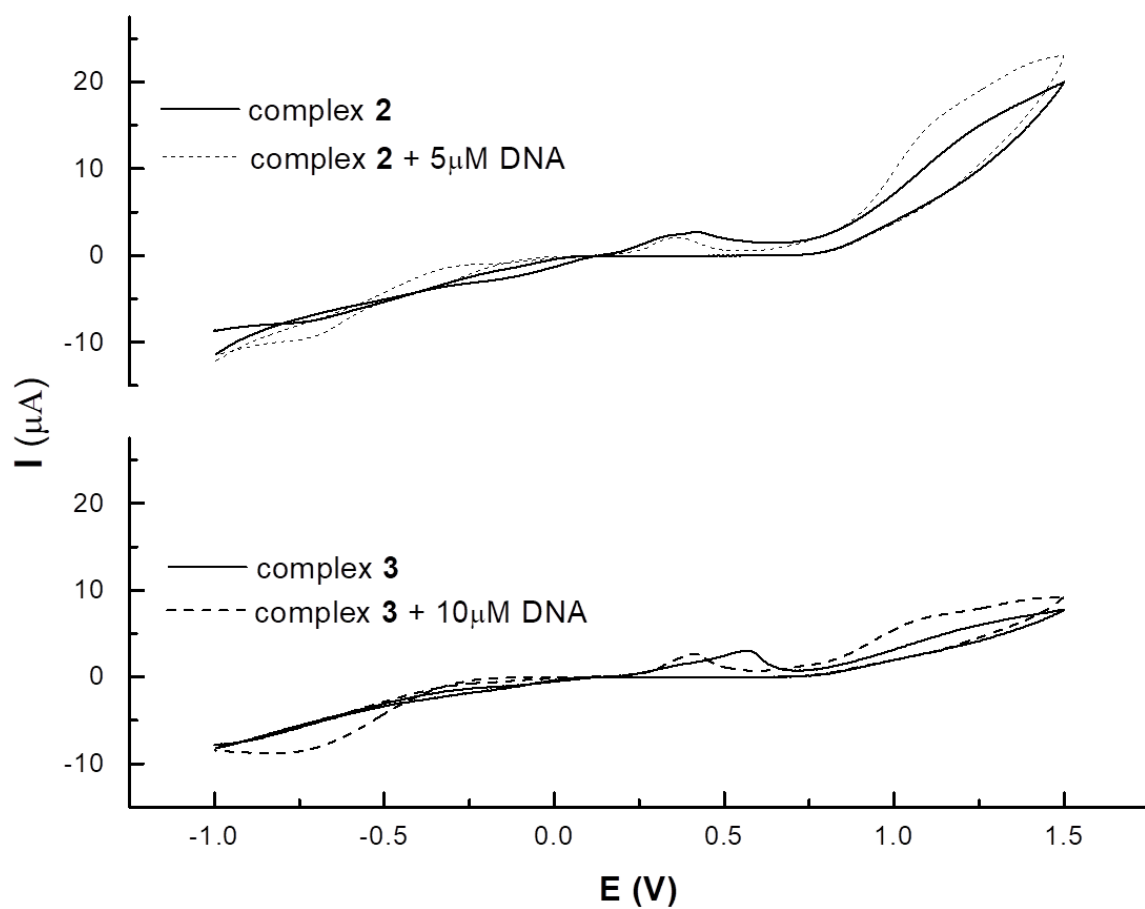


Fig. S11 CV voltammograms of complexes **2** and **3** after addition of increasing concentration of DNA.

Table S1 Selected bond distances (Å) and valence angles (°) in silver(I) complexes **1** – **3**.

1		2		3	
Ag1—N1	2.618(3)	Ag—N1	2.4978(15)	Ag1—N1	2.447(2) [2.479(2)] ^a
Ag1—N2	2.614(3)	Ag—N2'	2.7068(16)	Ag1—N5	2.255(2) [2.250(2)]
Ag1—N5	2.280(3)	Ag—N3	2.2924(15)	Ag1—N6	2.1829(19) [2.2057(19)]
Ag1—N6	2.279(3)	Ag—N4	2.2469(14)	Ag2—N3	2.489(2) [2.460(2)]
Ag2—N3	2.550(3)	Ag—O1	2.5978(15)	Ag2—N7	2.255(2) [2.255(2)]
Ag2—N7	2.278(3)			Ag2—N8	2.2055(19) [2.2004(19)]
Ag2—N8	2.260(3)				
Ag1—O1	2.612(3)				
Ag2—O1	2.594(3)				
N2—Ag1—N1	70.39(10)	N3—Ag—N1	73.69(5)	N5—Ag1—N1	75.40(7) [73.05(7)]
N1—Ag1—O1	118.92(9)	N4—Ag—N1	134.62(4)	N6—Ag1—N1	130.62(7) [136.06(7)]
N5—Ag1—N1	72.20(11)	N4—Ag—N3	131.01(5)	N6—Ag1—N5	149.80(7) [140.10(7)]
N5—Ag1—N2	142.57(10)	N1—Ag—O1	113.99(4)	N7—Ag2—N3	73.48(7) [74.06(7)]
N6—Ag1—N1	133.98(10)	N3—Ag—O1	85.16(5)	N8—Ag2—N3	136.08(7) [134.88(7)]
N6—Ag1—N2	70.20(10)	N4—Ag—O1	106.41(5)	N8—Ag2—N7	140.13(7) [141.05(7)]
N6—Ag1—N5	141.38(11)	N2'—Ag—O1	124.55(4)		
N6—Ag1—O1	94.09(10)	N2'—Ag—N3	140.52(4)	C1—N1—Ag1	112.04(12) [106.72(13)]
N2—Ag1—O1	105.96(9)	N1—Ag—N2'	70.53(4)	C10—N1—Ag1	113.22(13) [116.38(13)]
N5—Ag1—O1	93.10(10)	N2'—Ag—N4	69.99(4)	C11—N1—Ag1	102.35(13) [102.31(13)]
N3—Ag2—O1	108.83(9)	S—O1—Ag	129.91(7)	C5—N3—Ag2	115.73(13) [114.00(13)]
N7—Ag2—O1	98.05(10)	C1—N1—Ag	113.67(8)	C6—N3—Ag2	106.23(13) [108.39(12)]
N7—Ag2—N3	71.65(10)	C5—N1—Ag	107.06(8)	C23—N3—Ag2	103.72(13) [103.56(13)]
N8—Ag2—O1	90.20(11)	C6—N1—Ag	105.15(9)	C12—N5—Ag1	115.30(15) [116.80(15)]
N8—Ag2—N3	142.23(10)	C4'—N2'—Ag	108.9(8)	C16—N5—Ag1	125.00(16) [123.85(15)]
N8—Ag2—N7	139.26(11)	C12—N2'—Ag	89.88(8)	C18—N6—Ag1	118.62(14) [116.36(15)]
N9—O1—Ag2	116.80(2)	C7—N3—Ag	117.77(10)	C22—N6—Ag1	122.60(15) [124.68(15)]
C1—N1—Ag1	100.90(2)	C11—N3—Ag	122.77(11)	C24—N7—Ag2	118.08(15) [117.34(15)]
N9—O1—Ag1	112.9(2)	C(17)—N4—Ag	125.14(10)	C28—N—Ag2	123.18(15) [124.12(15)]

Ag1—O1—Ag2	127.24(10)	C13—N4—Ag	115.85(9)	C30—N8—Ag2	116.88(15) [117.26(14)]
C10—N1—Ag1	122.3(2)			C34—N8—Ag2	124.26(16) [123.82(15)]
C11—N1—Ag1	97.9(2)				
C2—N2—Ag1	109.9(2)				
C3—N2—Ag1	113.0(2)				
C17—N2—Ag1	100.19(19)				
C5—N3—Ag2	110.94(19)				
C6—N3—Ag2	112.0(2)				
C23—N3—Ag2	101.10(2)				
C12—N5—Ag1	117.2(2)				
C16—N5—Ag1	123.3(3)				
C18—N6—Ag1	120.2(2)				
C22—N6—Ag1	121.1(2)				
C24—N7—Ag2	117.8(2)				
C28—N7—Ag2	123.7(3)				
C30—N8—Ag2	118.3(2)				
C34—N8—Ag2	121.9(3)				

¹ refers to 1-x, 2-y, -z;

^avalues in square brackets refer to the second independent molecule

Table S2 Minimal biofilm inhibition (MBIC) and eradication concentrations (MBEC) of complexes **1** and **3**, μM (comparison between crystal violet and tetrazolium salt (XTT) assay is presented)

Assay	Crystal violet		XTT		
	1	3	1	3	
Test organism					
<i>C. albicans</i> ATCC 10231	MBIC	21.4 \pm 0.8	26.2 \pm 0.4	24.2 \pm 0.8	28.4 \pm 0.2
	MBEC	213.9 \pm 0.5	209.6 \pm 0.9	220.8 \pm 0.5	209.6 \pm 0.5
<i>C. albicans</i> 24 (isolate)	MBIC	26.7 \pm 0.4	26.2 \pm 0.2	25.5 \pm 0.4	25.2 \pm 0.4
	MBEC	>213.9 \pm 0.8	>209.6 \pm 0.8	>213.9 \pm 0.8	>209.6 \pm 0.6
<i>C. parapsilosis</i> ATCC 22019	MBIC	13.4 \pm 0.6	13.1 \pm 0.5	15.3 \pm 0.6	15.8 \pm 0.3
	MBEC	>213.9 \pm 0.4	>209.6 \pm 0.9	>213.9 \pm 0.4	>209.6 \pm 0.9

Table S3 Details of the crystal structure determinations of the silver(I) complexes **1** – **3**.

	1	2	3
Empirical formula	C ₃₄ H _{47.4} Ag ₂ N ₁₀ O _{7.7}	C ₃₆ H ₄₄ Ag ₂ F ₆ N ₈ O ₆ S ₂	C ₃₄ H ₄₄ Ag ₂ B ₂ F ₈ N ₈
CCDC number	1985892	1985893	1985894
Formula weight (g mol ⁻¹)	934.88	1078.65	954.13
Crystal system, space group	triclinic, <i>P</i> -1	monoclinic, <i>P</i> 2 ₁ / <i>n</i>	triclinic, <i>P</i> -1
<i>a</i> (Å)	8.935(5)	9.711(5)	12.418(7)
<i>b</i> (Å)	13.293(7)	14.665(7)	15.957(8)
<i>c</i> (Å)	17.094(8)	14.596(7)	19.137(9)
α (°)	68.521(16)		91.450(13)
β (°)	89.266(8)	95.032(10)	104.008(12)
γ (°)	80.532(7)		93.344(10)
<i>V</i> (Å ³)	1861.1(17)	2070.6(17)	3670(3)
<i>F</i> ₀₀₀	954	1088	1920
<i>Z</i>	2	2	4
X-radiation, λ /Å	Mo- <i>K</i> _{α} 0.71073	Mo- <i>K</i> _{α} 0.71073	Mo- <i>K</i> _{α} 0.71073
data collect. temperat. /K	100(1)	100(1)	100(1)
Calculated density (Mg m ⁻³)	1.668	1.730	1.727
Absorption coefficient (mm ⁻¹)	1.116	1.129	1.147
Crystal size (mm ³)	0.16 × 0.10 × 0.08	0.33 × 0.19 × 0.15	0.23 × 0.20 × 0.19
θ range (°)	2.3 to 26.4	2.0 to 32.4	1.3 to 32.5
index ranges <i>h, k, l</i>	-11 ... 11, -16 ... 16, -21 ... 21	-14 ... 14, -21 ... 22, -21 ... 21	-18 ... 18, -23 ... 23, -28 ... 28
No. of collected and independent reflections	35151, 7621	52271, 7121	95349, 24637
<i>R</i> _{int}	0.0560	0.0344	0.0493
Data / restraints / parameters	7621 / 6 / 530	7121 / 0 / 271	24637 / 413 / 1019
Goodness-on-fit on <i>F</i> ²	1.030	1.064	1.030
Final <i>R</i> indices [<i>F</i> _o > 4 σ (<i>F</i> _o)] <i>R</i> (<i>F</i>), <i>wR</i> (<i>F</i> ²)	0.0352, 0.0767	0.0239, 0.0620	0.0374, 0.0730
Final <i>R</i> indices (all data) <i>R</i> (<i>F</i>), <i>wR</i> (<i>F</i> ²)	0.0556, 0.0856	0.0296, 0.0645	0.0635, 0.0828
Difference density: max, min (e Å ⁻³)	1.854, -0.522	0.779, -0.275	1.348, -0.825